A REVIEW ON DISCRETE FILTERING TOOLS FOR TRUSS OPTIMIZATION

Maurílio de Jesus Souza

Sylvia Regina Mesquita de Almeida

maurilio.engcivil@gmail.com

sylviaalm@gmail.com

Escola de Engenharia Civil e Ambiental Universidade Federal de Goiás

Av. Universitária no. 1488, Setor Universitário, 74605-220, Goiânia. Goiás, Brazil

Abstract. *The ground structure method is based on a size optimization of highly connected trusses. The design solution is extracted in a post-processing step by filtering out the unnecessary thin bars. Recently filters have been proposed to extract a topology in equilibrium at each step in order to obtain clearly defined structures in equilibrium during the topology optimization process. This paper reviews the discrete and the maximum filter approaches and proposes improvements in the filtering technique. Examples are provided to demonstrate the capabilities of each approach.*

Keywords: *Truss Optimization, Topology Optimization, Ground Structure Method, Filter*

1 INTRODUCTION

The Ground Structure Method (GSM) was first developed by Dorn et. al. (1964) to provide approximations to optimal Michell trusses (Hemp, 1973) and today is highly used in the field of Topology Optimization (TO). The generation structural layouts is based on a size optimization process applied to a dense and highly interconnected initial truss structure with fixed nodes (ground structure). Figure 1 illustrates the process for a cantilever beam with a single mid-height point load at the free end as shown in Fig. 1(a) to which the full connected ground structure shown in Fig. 1(b) is associated. In the standard approach, the optimization process sets a small value to the unnecessary members and at the end of the optimization process lots of thin members remains in the structure, as shown in Fig. 1(c). The topology is extracted at the end of the process by removing the resultant thin members (Fig. 1(d)).

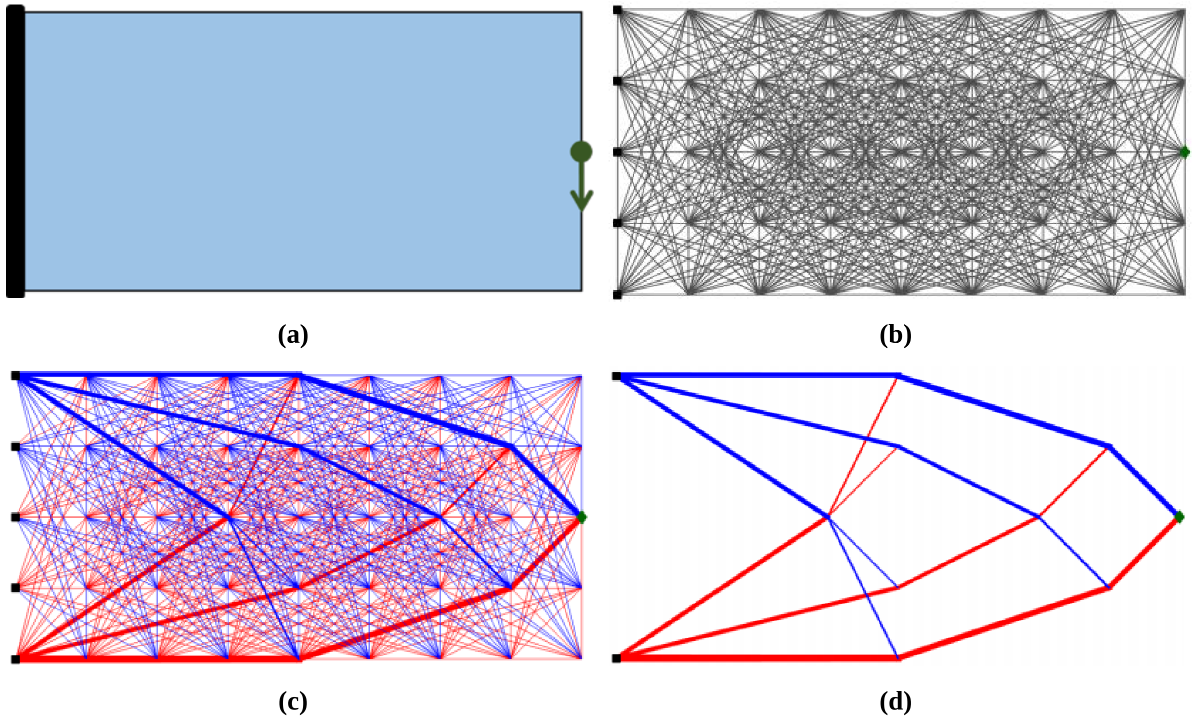

Figure 1. Application of the GSM to a cantilever beam: (a) domain and boundary conditions; (b) initial ground structure; (c) optimal structure after sizing optimization; (d) final topology.

Recently filters proposed by Ramos Jr and Paulino (2016) and by Sanders et al (2017) have made the transition of the ground structure approach form a size optimization process with topology extraction to an actual topology optimization process. The two papers mentioned above propose filters to extract the topology form the ground structure during the optimization process and apply the technique to the so called compliance problem. Ramos e Paulino (2016) use a constant filter to eliminate the bars with area bellow the filter value while checking at each configuration the equilibrium of the extracted topology. Sanders et al (2017) seeks for the maximum value of the filter to be applied at each step of the optimization process. The topology extraction causes an increase in the compliance value and conduces to less bars in the final structural layouts. However, both techniques allow to control this jump in order to preserve some thin bars in order to obtain more complex layouts.

This paper compares the two filters proposed by Ramos Jr e Paulino (2016) and Sanders et al (2017) specially with respect to the compliance control. An improvement on the search for the maximum filter is also proposed. This paper is organized as follows: Section 2 discusses presents the topology optimization approaches, including formulations and flowcharts. Section 3 presents the numerical examples and conclusions are presented in Section 4.

2 FORMULATION

This section presents the standard elastic formulation of the ground structure method followed by the constant filter for the elastic formulation and the maximum filter for the elastic and for the plastic formulations. An improvement in the maximum filter for both elastic and plastic formulations are presented on the correspondent item.

2.1 Standard elastic formulation

The classical nested elastic formulation is usually adopted in optimization associated with the ground structure method. In this work, the optimization problem is to find the vector of cross-sectional areas (**x**) of a truss structure, with compliance minimization, subject to a volume constraint, which is similar to the compliance problem in topology optimization with density method. Christensen and Klarbring (2009) showed that this problem is similar equivalent to minimizing the volume with compliance constraint.

$$
\begin{aligned}
\min_{\mathbf{x}} \quad & C(\mathbf{x}) = \mathbf{F}^T \mathbf{u}(\mathbf{x}) \\
s.t. \quad & \mathbf{L}^T \mathbf{x} \le V^{\max} \\
& x_i^{\min} \le x_i \le x_i^{\max} \\
with \quad & \mathbf{K}(\mathbf{x})\,\mathbf{u}(\mathbf{x}) = \mathbf{F}
\end{aligned}
\tag{1}
$$

where C is the structural mean compliance, **F** are the external forces, **u** are nodal displacements (state variables), **L** are the member lengths, $V^{\max}$ is the maximum volume, $x_i^{\min}$ and $x_i^{\max}$ are the lower and upper bounds on member cross-sectional areas, respectively, and **K** is the global stiffness matrix.

During the optimization process, most member cross-sectional areas tend to zero. Thus, in formulation (1) the lower bound $x_i^{\min}$ is set as a small positive number to avoid a singular or ill-conditioned stiffness matrix. Therefore, the final (optimal) structure contains all members originally present in the ground structure, classifying Eq. (1) as a sizing optimization problem. To extract the topology using the formulation in Eq. (1), a cutoff is commonly applied to the final structure, eliminating thin members and maintaining only those whose normalized cross-sectional areas are greater than a chosen value α_f. The Cutoff criterion is presented in Eq. (2) and illustrated by Fig. 2. Depending on the cutoff level adopted lots of thin bars can remain in the structural design or the extracted topology may not match the equilibrium.

$$x_i = Cutoff\,(\mathbf{x}, \alpha_f) = \begin{cases} 0 & if\ \dfrac{x_i}{\max(\mathbf{x})} < \alpha_f \\ x_i & otherwise \end{cases} \tag{2}$$

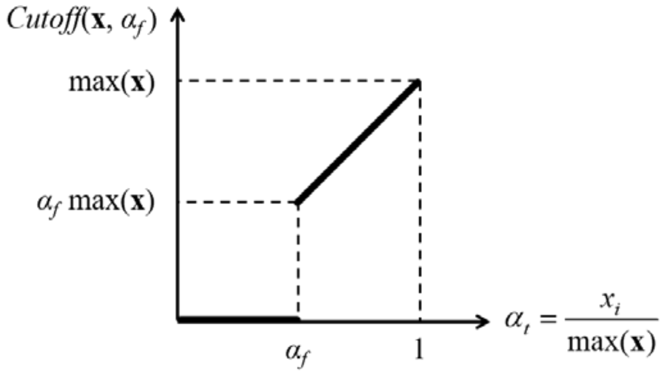

Figure 2. Illustration of the Cutoff.

In the problem set on Eq. (1) the sensitivity of the compliance with respect to the desin variable *i* is given by Eq. (3), where $\mathbf{K}_i^0$ is the basic stiffness matrix for element *i*. Equation (3) shows that the sensitivity of a member does not depend on the its cross-sectional area and is always non-positive. More information about sensitivity analysis can be found in Christensen and Klarbring (2009) and Ohsaki (2010).

$$\frac{\partial C(\mathbf{x})}{\partial x_i} = -\mathbf{u}(\mathbf{x})^T \mathbf{K}_i^0 \mathbf{u}(\mathbf{x}) \tag{3}$$

2.2 Constant filter

Ramos Jr. and Paulino (2016) introduced a discrete filter (hereinafter called constant filter) to extract topologies in equilibrium from the ground structure during the optimization process. By this approach a predetermined (constant) filter value is applied in every iteration of the optimization process. Because the filtering scheme allows members to be removed from the ground structure, the structural problem may become singular and the global equilibrium may be violated. To avoid singularities Ramos Jr. and Paulino (2016) apply a Tikhonov regularization (TR) (Tikhonov and Arsenin, 1977) to the total potential energy of the system. Therefore, the regularized optimization problem is written as:

$$\begin{aligned} &\min_{\mathbf{x}} && C(\mathbf{x}) = \mathbf{F}^T \mathbf{u}(\mathbf{x}) \\ &s.t. && \mathbf{L}^T \mathbf{x} \le V^{\max} \\ & && 0 \le x_i \le x_i^{\max} \\ &with && Filter(\mathbf{x}, \alpha_f) \\ &and && \min_{\mathbf{u}}\ \Pi(\mathbf{u}(\mathbf{x})) + \frac{\lambda}{2}\mathbf{u}(\mathbf{x})^T \mathbf{u}(\mathbf{x}) \end{aligned} \tag{4}$$

where *Filter* follows the same idea of the Cutoff presented in Eq. (2) and Fig. 2, Π is the total potential energy of the system (defined in Eq. (5)) and the last term of the last state equation in (4) represents the Tikhonov regularization, where λ is the Tikhonov parameter.

$$\Pi(\mathbf{u}(\mathbf{x})) = \frac{1}{2}\mathbf{u}(\mathbf{x})^T \mathbf{K}(\mathbf{x})\mathbf{u}(\mathbf{x}) - \mathbf{F}^T \mathbf{u}(\mathbf{x}) \tag{5}$$

The new singular structural problem is then written as in Eq. (6), where for the Tikhonov parameter λ is often assigned a small value, say 10^{-8} to 10^{-12} times the mean of the diagonal of **K**, and **I** is the identity matrix.

$$(\mathbf{K}(\mathbf{x}) - \lambda \mathbf{I})\mathbf{u}(\mathbf{x}) = \mathbf{F} \tag{6}$$

For the topology equilibrium check, the global equilibrium residual R is used, as shown in Eq. (7), where ρ is the equilibrium tolerance parameter.

$$R = \frac{\|\mathbf{Ku} - \mathbf{F}\|}{\|\mathbf{F}\|} \leq \rho \tag{7}$$

In addition to the global equilibrium check, the variation of the objective function (i.e., compliance) between consecutive iterations (k-1 to k) may be controlled. The variation ΔC is calculated as in Eq. (8) and should not be greater than the tolerance *ObjTol*.

$$\Delta C = \frac{C^k - C^{k-1}}{C^{k-1}} < ObjTol \tag{8}$$

Both the equilibrium and objective variation control tests are made together for the current topology. If one of them fails, adjustments are made in the Optimality Criteria algorithm in order to adjust the search region and seek for new design variables values, namely the multiplier parameter γ, which defines the move limit M, set as in Eq. (9) at the beginning of the optimization process.

$$M = \gamma\, x_0 \tag{9}$$

Ramos Jr e Paulino (2016) claim that in the constant filter approach the user has total control over the final topologies, as he/she chooses the filter value to be applied (and consequently the ratio between the minimum and maximum member areas that belong to the topology) and limits how the objective function graph will converge. If a large value is assigned to the filter, however, a topology in equilibrium might not be found.

Figure 3 illustrates the optimization problem for the constant filter formulation in Eq. (4), calling attention to the regular optimization loop at the left side of the figure and to the additional loop in the right side related to the compliance control.

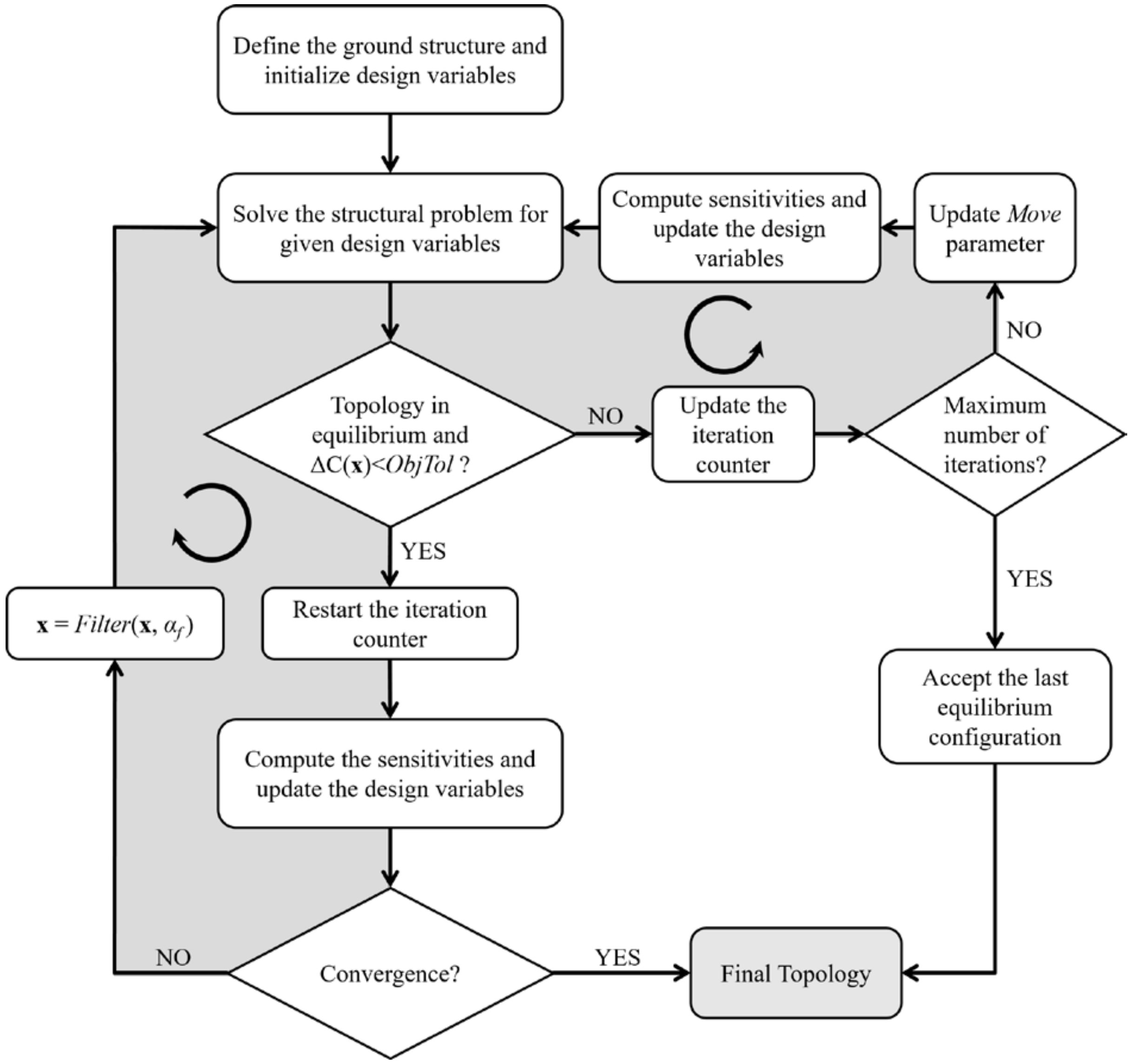

Figure 3. Flowchart of the optimization problem with constant filter approach. (adapted from Ramos Jr; Paulino, 2016)

2.3 Maximum filter

In the constant filter approach the user is challenged to select a good filter value to be applied in every iteration of the optimization process: it should be large enough to remove unnecessary thin members, and small enough to keep structural important bars that lead to a topology in equilibrium. Besides, in some iterations, the specified filter value might cause large jumps in the objective function, disrupting a smooth convergence process. To avoid the aforementioned drawbacks, Sanders et al. (2017) developed the bisection scheme shown in Fig. 4 to determine, at every iteration, the maximum allowed filter value that maintains the global equilibrium of the filtered structure and do not violate the prescribed tolerance for the change in the objective. The optimization problem for the maximum filter approach is equal to (4) in constant filter, except for the *Filter* step.

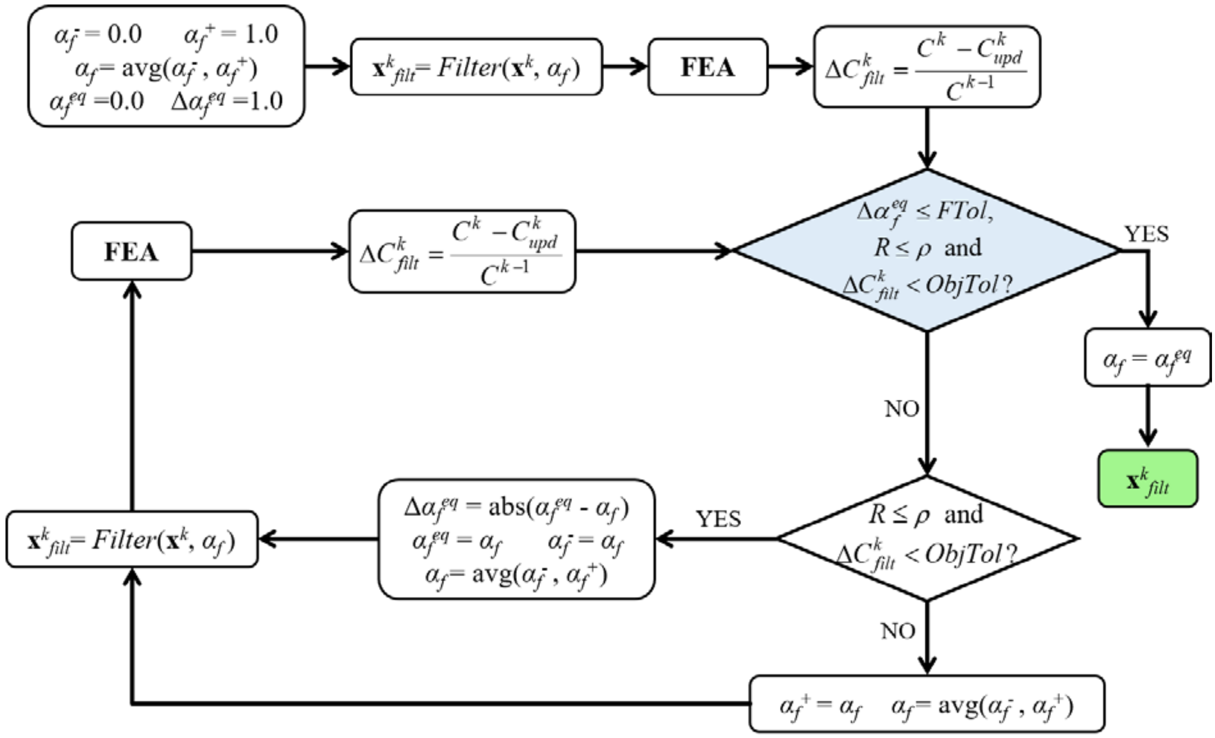

Figure 4. Flowchart of the bisection scheme to search the maximum filter in each iteration. (adapted from Sanders et al., 2017)

In the maximum filter approach the filter application may be imposed at each N_f iterations rather than at every iteration. Furthermore, the variation in compliance right after the design variable update (C^k_{upd}) may be limited by the designer. This variation is calculated according to Eq. (10) and is illustrated in Fig. 5. in which: point **a** represents the compliance value at the end of iteration k-1; point **b** represents the compliance value after design variable update in iteration k; and point **c** represents the compliance value after the filter is imposed in iteration k, which is increased from point **b** such that ΔC^k_{filt} is less than the prescribed tolerance ($ObjTol$).

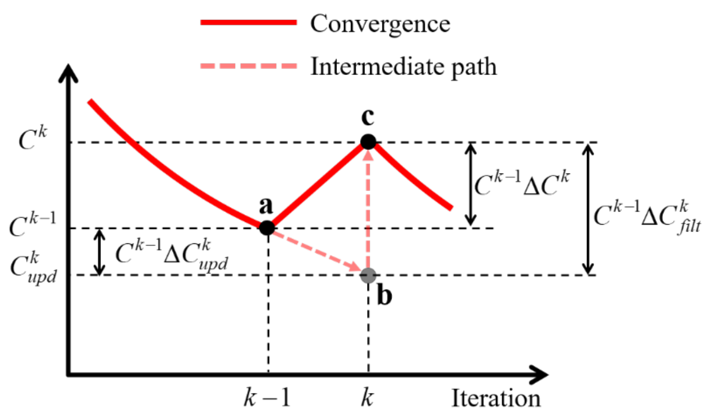

Figure 5. Demonstration of the variation of the objective function from iteration k-1 to iteration k. (adapted from Sanders et al., 2017)

$$\Delta C_{filt}^{k} = \frac{C^{k} - C_{upd}^{k}}{C^{k-1}} < ObjTol \tag{10}$$

In the bisection scheme proposed by Sanders et al. (2017), a Finite Element Analysis (FEA) is performed for every filter value tested in the current iteration of the optimization process until the filter convergence is met, and the global equilibrium residual and objective function variation have attended their respective tolerances. However, it may happen that, for consecutively filter values tested, the exactly same current topology is found, or an alternation between a topology in equilibrium and another in non-equilibrium. Thus, to prevent redundant finite element analysis, we propose here an improved bisection scheme (Fig. 6) in which the number of bars of the new topology is tested before the FEA is performed. If the current topology is the same as one of those already tested, no FEA is needed. This improvement in the implementation may represent significant computational savings, especially for ground structures with a large number of bars.

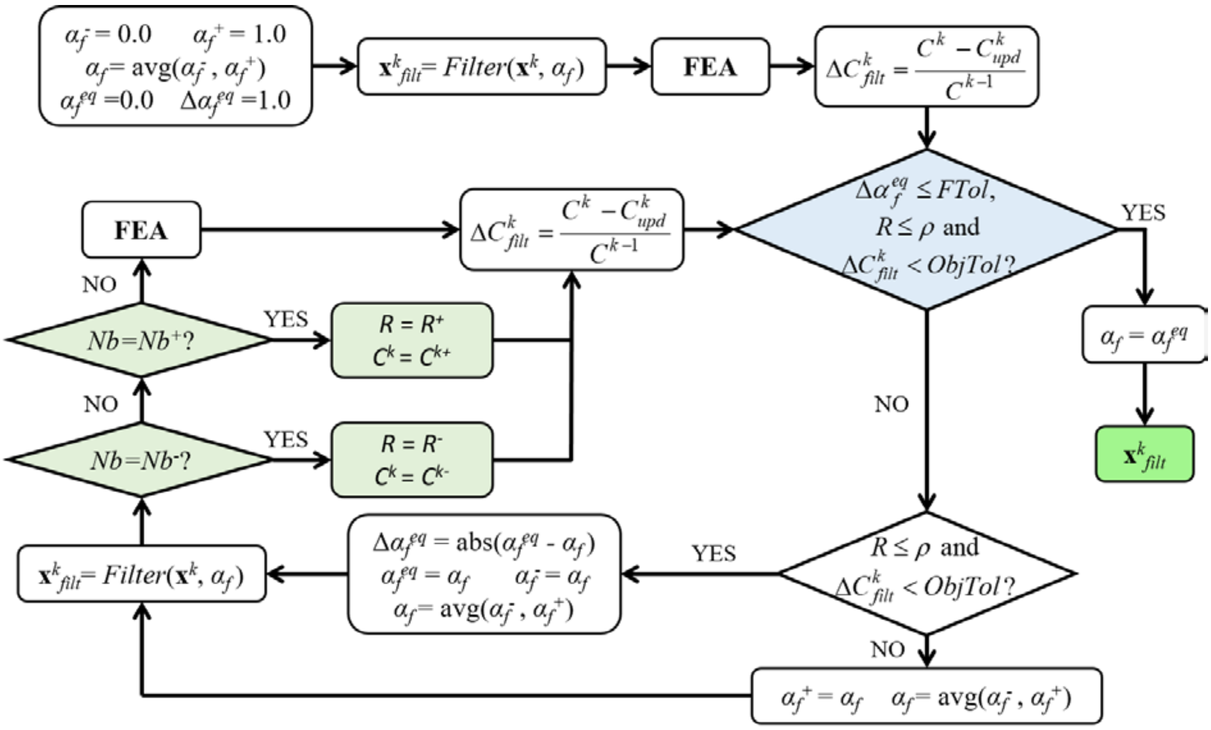

Figure 6. Flowchart of the improved bisection scheme to search the maximum filter in each iteration.

Furthermore, the maximum filter approach can also be adopted at the end of the optimization process (after either standard elastic optimization or maximum end filter optimization), as a maximum end filter. In these cases, a new tolerance for the variation of objective at the end (*EndObjTol*) might be chosen.

2.4 Maximum end filter for plastic formulation

The idea of the maximum end filter explained in the previous section can be further applied to the truss optimization with plastic formulation. The formulation based on plastic analysis seeks to minimize the total structural volume (V) enforcing the equilibrium of forces (no

Proceedings of the XXXVIII Iberian Latin-American Congress on Computational Methods in Engineering
P.O. Faria, R.H. Lopez, L.F.F. Miguel, W.J.S. Gomes, M. Noronha (Editors), ABMEC, Florianópolis, SC, Brazil, November 5-8, 2017.

compatibility or stress-strain relations) through the nodal equilibrium matrix **B**, and stress constrains (transformed to force constrains):

$$\begin{aligned} \min_{\mathbf{x}} \quad & V = \mathbf{L}^T \mathbf{x} \\ s.t. \quad & \mathbf{B}^T \mathbf{N} = \mathbf{F} \\ & -\sigma_C x_i \le N_i \le \sigma_T x_i \end{aligned} \tag{11}$$

where **N** is the vector of internal forces of all ground structure members, and σ_C and σ_T are the stress limits in compression and tension, respectively.

According to formulation in Eq. (11), the stress constrains in both tension and compression must be actives for all members at the optimal solution, since, if a member constrain is not active, its area can always be reduced (reducing the structure volume) without violating the constrains. It means the optimal structure is always *fully stressed*.

Using the slack variables $\mathbf{s}^+$ and $\mathbf{s}^-$, the optimization problem (11) can be transformed into the linear programming problem (12), where V^* is the total volume calculated for $\sigma_T = 1$. This new problem may be efficiently solved using the interior-point algorithm (Zegard; Paulino, 2014).

$$\begin{aligned} \min_{\mathbf{s}^+, \mathbf{s}^-} \quad & V^* = \frac{V}{\sigma_T} = \mathbf{L}^T(\mathbf{s}^+ + \kappa \mathbf{s}^-) \\ s.t. \quad & \mathbf{B}^T(\mathbf{s}^+ - \mathbf{s}^-) = \mathbf{F} \\ & s_i^+, s_i^- \ge 0 \end{aligned} \tag{12}$$

Figure 7 shows the flowchart of the algorithm for the plastic formulation in which a maximum end filter technique is applied.

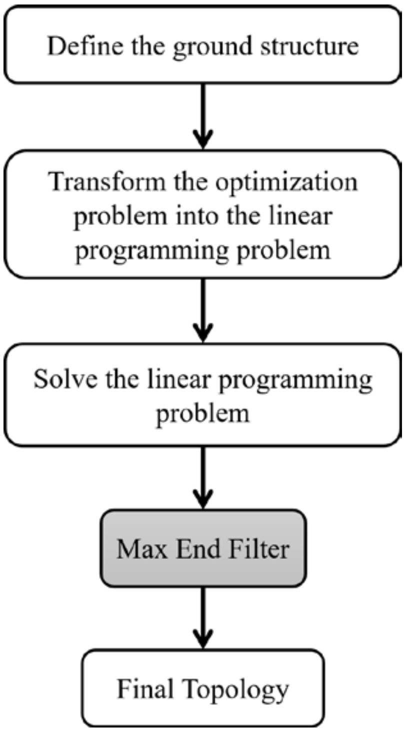

Figure 7. Flowchart of the algorithm for the maximum end filter with plastic formulation.

3 NUMERICAL EXAMPLES

Numerical examples are provided below to illustrate the features of the filtering tools discussed in the previous section. In the first example, we apply the constant filter and the max filter approaches to a rectangular cantilever beam, while in the second example we use the plastic formulation with a maximum end filter in a 3D shell structure.

For all examples, the collinearity parameter is *ColTol* = 0.999999 and the Tikhonov parameter $\lambda_0 = 10^{-12}$. In the examples that uses elastic formulation, the lower and upper bounds for the design variables are set as $x_i^{\min} = 0$ and $x_i^{\max} = 10^4\,x_0$, respectively. In all topologies, *blue* indicates tension while *red* indicates compression. Finally, a post-processing step to delete aligned nodes was performed for the final topologies in all examples.

3.1 Example 1 – Cantilever beam

The first example, illustrated by Fig. 8, consists of a rectangular cantilever beam (L = 8 m; H = 5 m) with a concentrated load P = 100 kN applied at mid-height of the right end. The full level ground structure used here (Fig. 8(b)) is constructed with a grid of 11x9 nodes, resulting in 3026 non-overlapping bars. The maximum total structural volume is set as $V^{\max} = 0.0044$ m^3, and the lower and upper bounds are $x_i^{\min} = 0$ and $x_i^{\max} = 3.962\ 10^{-3}$ m^2, respectively. Furthermore, the convergence tolerance is $Tol = 10^{-10}$.

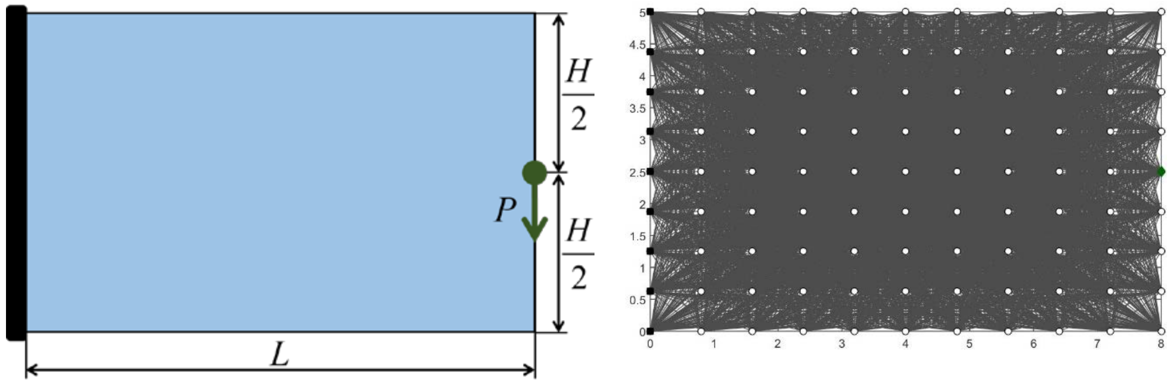

(a) **(b)**

Figure 8. Cantilever of Example 1: (a) design domain; (b) ground structure with 3026 bars.

3.1.1 Constant filter

The final topologies for this example using the constant filter are depicted in Fig. 9 for several filter values. In all cases the objective function convergence was not controlled ($C_{Tol} = \infty$). These results show that, as the filter value increases, topologies with fewer number of bars are obtained, as expected. Furthermore, all topologies are guaranteed to be in equilibrium.

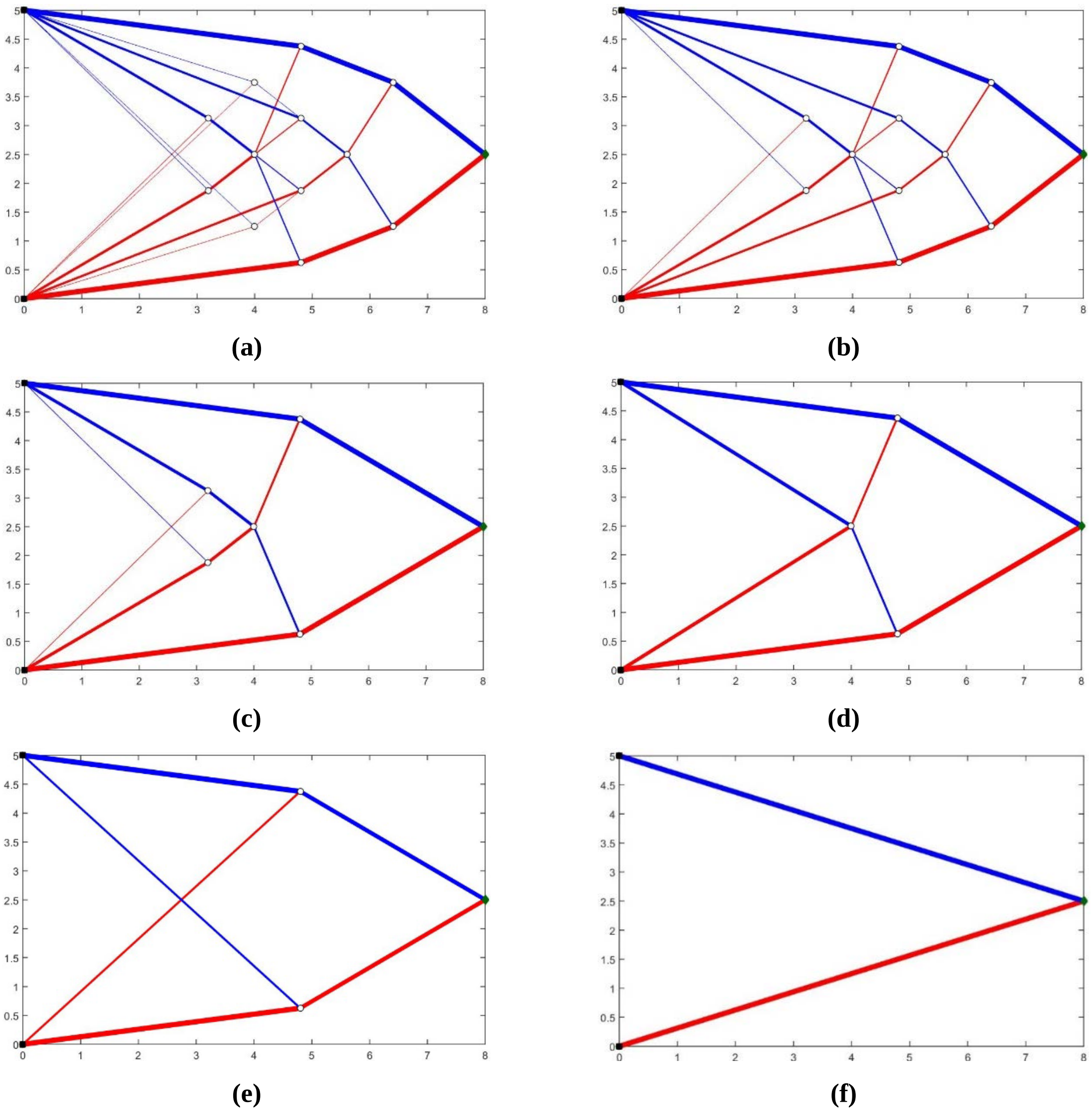

Figure 9. Final topologies for Example 1 using constant filter with objective control ($C_{Tol} = \infty$) and: (a) $\alpha_f = 10^{-6}$; (b) $\alpha_f = 10^{-4}$ (c) $\alpha_f = 0.05$; (d) $\alpha_f = 0.1$; (e) $\alpha_f = 0.4$; (f) $\alpha_f = 0.8$.

3.1.2 Maximum filter

For the maximum filter approach, different sets of the parameters N_f and C_{Tol} are applied. For all cases, we adopt the move parameter $\gamma = 0.8$ and the tolerance for the bisection scheme $FTol = 10^{-4}$. The following figures show the final topologies, along with the graphs of convergence and applied filter values, while the tables supply the numerical data of the optimization process.

Figure 10 shows the results obtained with decreasing values for the parameter of objective control C_{Tol} and application of maximum filter at every iteration of the optimization ($N_f = 1$). Table 1 presents the respective data results. As C_{Tol} is tighten up, the jumps in the objective function become smaller, restraining the filters to small values and resulting in topologies with higher number of bars. Moreover, the comparison of computational cost demonstrate that the improved approach was more efficient for this set of parameters and that the improvement rate decreases with the decrease of the C_{Tol} parameter.

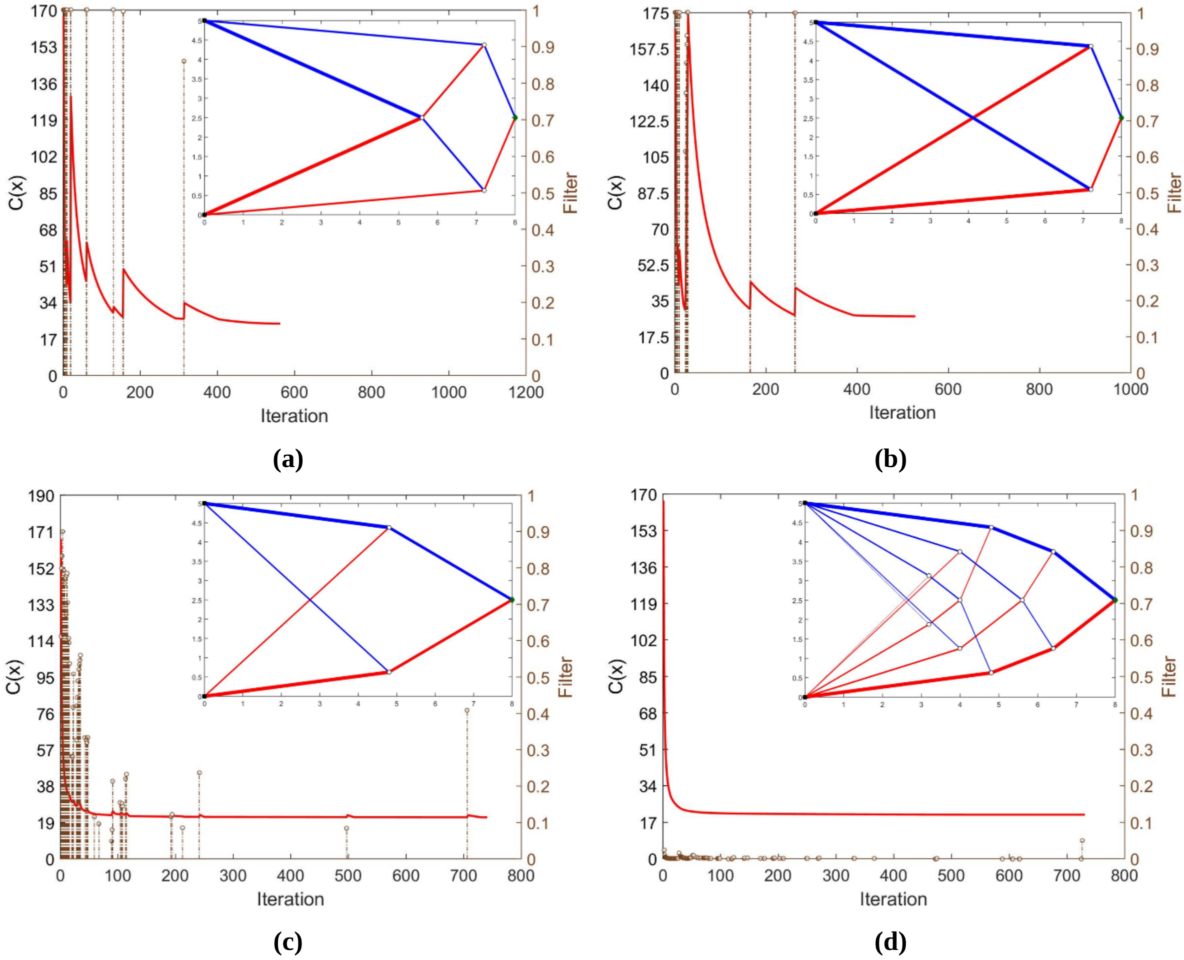

Figure 10. Results of Example 1 using maximum filter approach with N_f = 1 and: (a) $C_{Tol} = \infty$; (b) C_{Tol} = 0.5; (c) C_{Tol} = 0.05; (d) C_{Tol} = 0.0001.

Table 1. Gain of computational cost with the improved maximum filter approach for Example 1 with N_f = 1 and decreasing C_{Tol}.

C_{Tol}	C_{end} (kN.m)	Nb_{end}	*# Iter*	Max Filter time (s)	Imp Max Filter time (s)	Time improved
∞	24.1167	8	560	49.71	12.92	74.01 %
0.5	27.3826	6	525	44.41	11.26	74.64 %
0.05	21.7349	6	739	75.47	26.56	64.81 %
0.0001	20.5612	22	729	145.07	110.54	23.80 %

The next set of topologies were obtained by not restricting jumps in the compliance convergence ($C_{Tol} = \infty$) and by postponing the application of the maximum filter (increasing values for N_f). The topologies in Fig. 11 show that, as the parameter N_f increases, the final

Proceedings of the XXXVIII Iberian Latin-American Congress on Computational Methods in Engineering
P.O. Faria, R.H. Lopez, L.F.F. Miguel, W.J.S. Gomes, M. Noronha (Editors), ABMEC, Florianópolis, SC, Brazil, November 5-8, 2017.

topologies have higher number of bars, a pattern of results opposite to the previous case (N_f = 1 and decreasing C_{Tol}). Table 2 show that, as expected, if the filter application postponed too much, the improvements has little effect in the computational time.

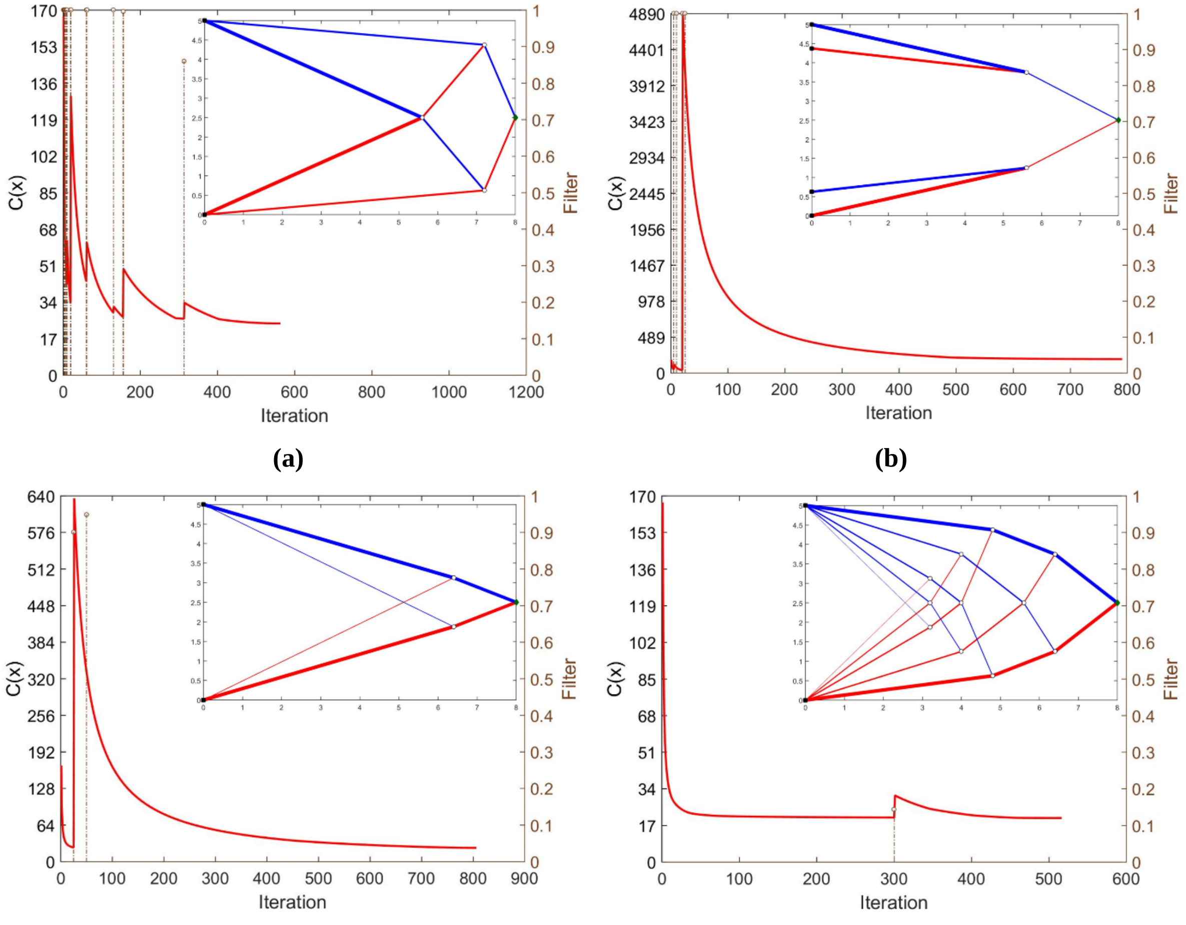

(a) (b) (c) (d)

Figure 11. Results of Example 1 using maximum filter approach with C_{Tol} = ∞ and: (a) N_f = 1; (b) N_f = 5; (c) N_f = 25; (d) N_f = 300.

Table 2. Gain of computational cost with the improved maximum filter approach for Example 1 with C_{Tol} = ∞ and increasing N_f.

N_f	C_{end} (kN.m)	Nb_{end}	*# Iter*	Max Filter time (s)	Imp Max Filter time (s)	Time improved
1	24.1167	8	560	49.71	12.92	74.01 %
5	188.894	6	789	18.96	10.32	45.57 %
25	24.1469	6	804	19.46	19.10	1.85 %
300	20.4757	24	515	129.30	143.21	___

Finally, Fig. 12 presents the final topologies obtained by avoiding jumps in the objective (C_{Tol} = 0.0001) and increasing the parameter N_f. As expected, topologies with higher number of bars are obtained. Similar to the previous case, the proposed improvement on maximum filter approach might not be worth it to use when the values of parameter N_f are high.

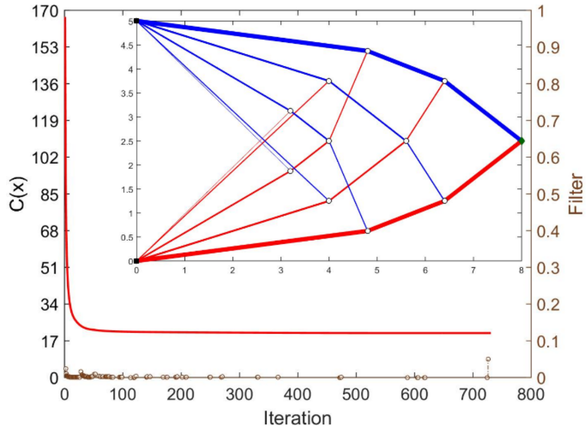

(a)

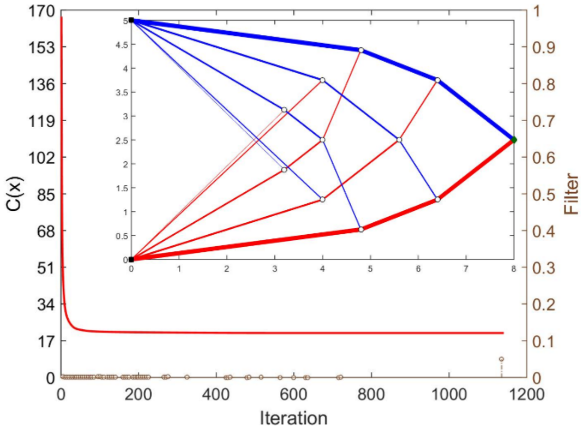

(b)

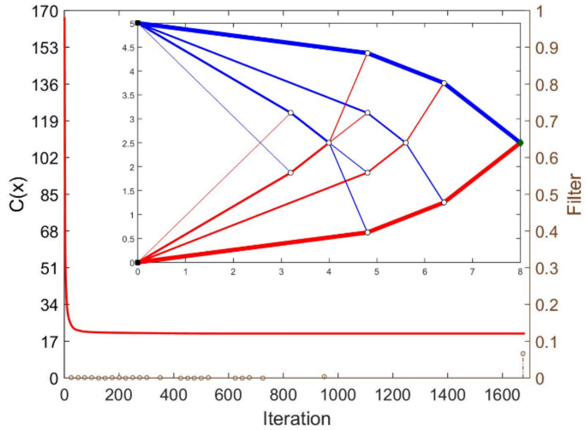

(c)

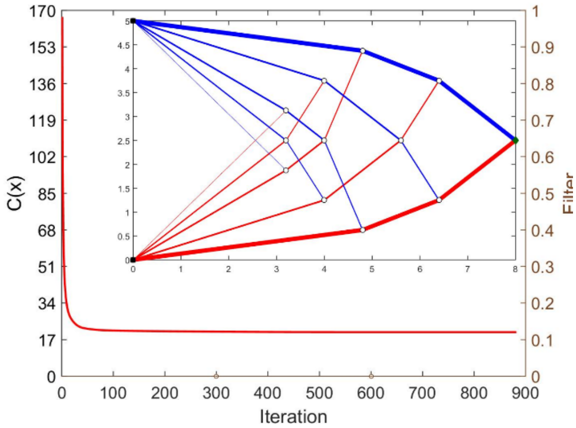

(d)

Figure 12. Results of Example 1 using maximum filter approach with C_{Tol} = 0.0001 and: (a) N_f = 1; (b) N_f = 5; (c) N_f = 25; (d) N_f = 300.

Table 3. Gain of computational cost with the improved maximum filter approach for Example 1 with C_{Tol} = 0.0001 and increasing N_f.

N_f	C_{end} (kN.m)	Nb_{end}	# *Iter*	Max Filter time (s)	Imp Max Filter time (s)	Time improved
1	20.5612	22	729	145.07	110.54	23.80 %
5	20.5612	22	1138	60.84	56.65	6.88 %
25	20.5312	22	1678	49.47	51.48	___
300	20.4761	24	880	139.57	152.60	___

3.2 Example 2 – Maximum end filter with plastic formulation

For this example, we analyze the shell structure with the format of half of one sheet hyperboloid with a total load of P = 100 kN applied at all nodes on top, as shown in Fig. 13(a). The domain simulates a tunnel structure, the dimensions are presented at the respective axis and the sum of all point loads is P = 100 kN. The dimensions of the central part of the structure are reduced 2/3 from dimensions at the borders. Despite not shown, the supports are present in all nodes at the base. Figure 13(b) depicts the ground structure used for this example, which has a connectivity level of 4, based on a node grid of (N_x,N_θ)=(10,10), resulting in 1770 non-overlapping bars.

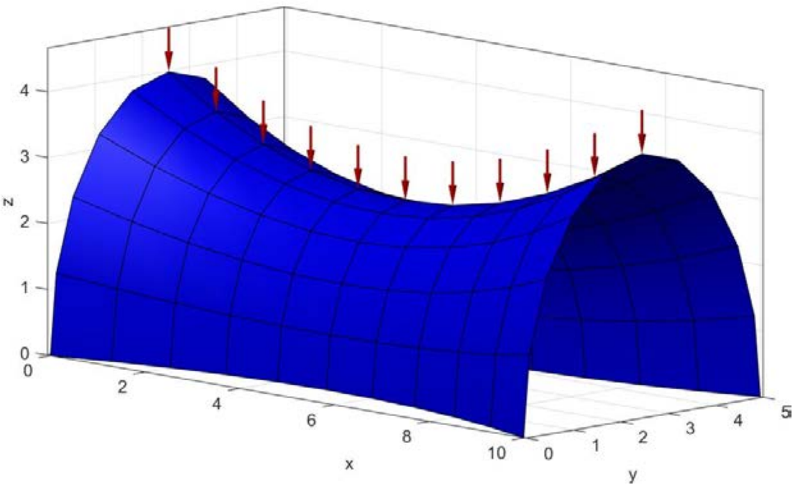

(a)

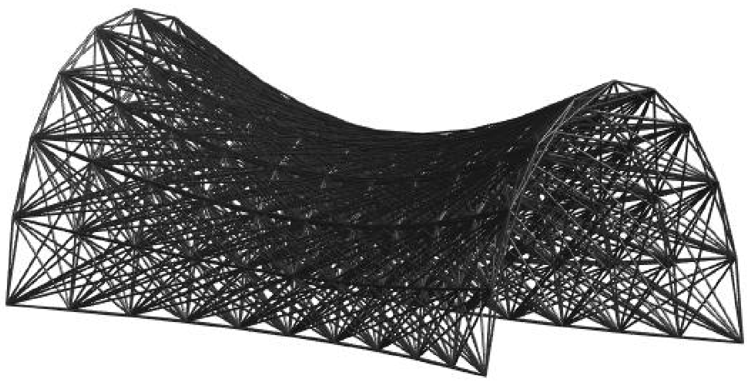

(b)

Figure 13. Shell structure of Example 2: (a) design domain; (b) initial ground structure with 1770 bars.

The plastic formulation with volume minimization and stress constrains is employed, and to the optimal structure we apply the maximum filter approach as a maximum end filter. We assume for the stress limits in tension and compression $\sigma_C = \sigma_T$ = 262 MPa (κ = 1).

Figure 14 shows the views of the final topology obtained with the application of an end filter of 0.01564. The total structural volume is V = 0.0084 m^3 and a full stress design is achieved, as expected.

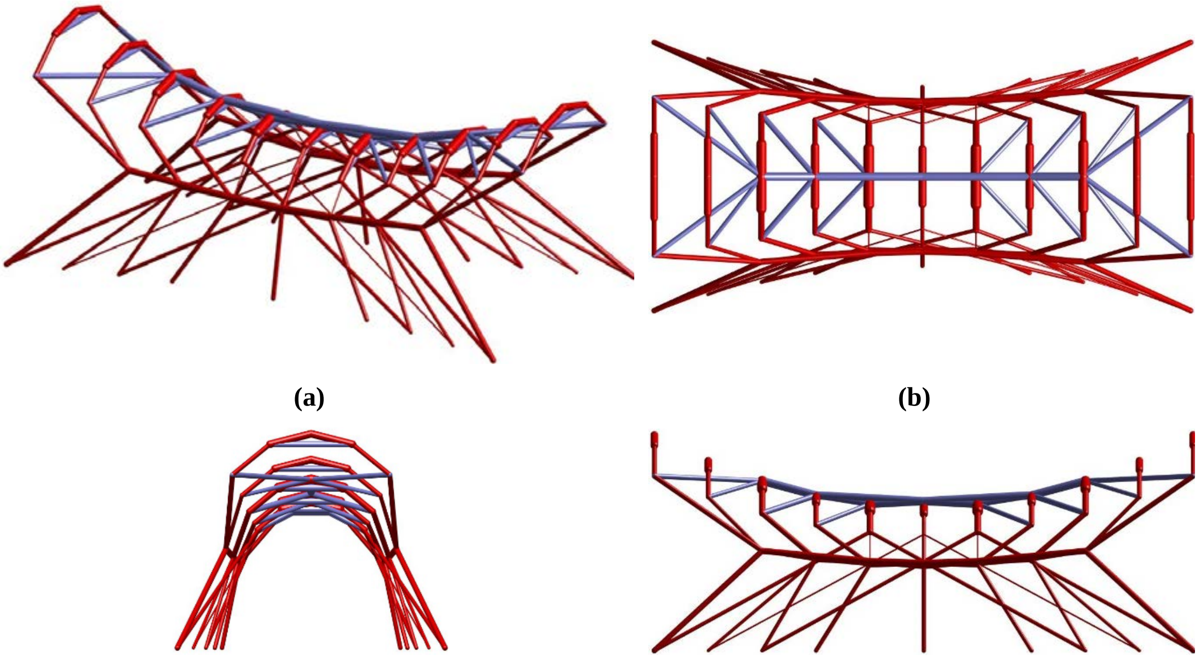

(a) (b)

(c) (d)

Figure 14. Final topology of Example 2 using plastic formulation with and end filter of 0.01564: (a) isometric view; (b) top view; (c) front view; (d) lateral view.

3.3 Example 3 – Bridge problem

The last example is the problem of a bridge with distributed pointed load at the base, as shown if Fig. 15(a), for which we utilize the maximum filter approach. Dimensions are H = 5 m and L = 10 m, and each load is P = 10 kN.

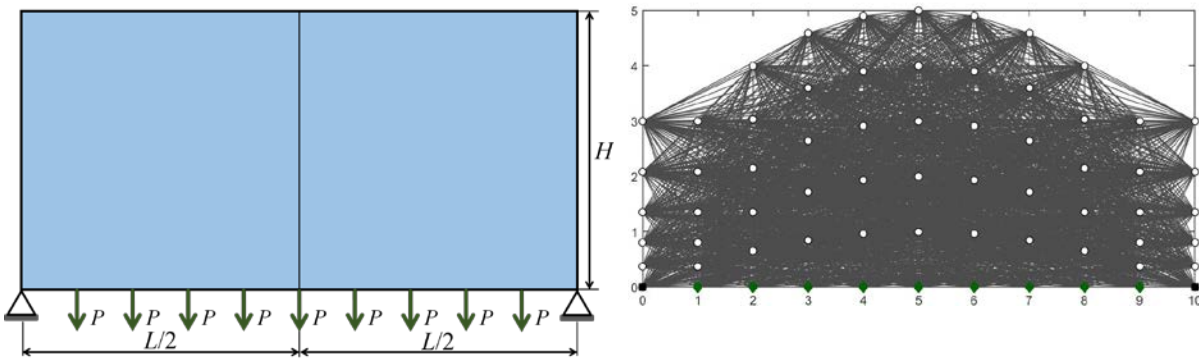

(a) (b)

Figure 15. Bridge of Example 3: (a) design domain; (b) initial ground structure (from modified grid) with 1944 bars.

The final topology expected for this bridge problem is an arch connecting both supports, from which hanging cables link the loads. However, the structured grid commonly used in the ground structure method will hardly provide a topology in which the bars form a smooth curvature to represent the arch. Thus, for this example we modify the positions of the nodes of a 11x6 structured node grid to form arches connecting the supports and the central nodes. The nodes above the supports have the same position in *y* axis of their right/left neighbors. This modified grid conduct to the level 10 ground structure in Fig. 15(b), containing 1944 non-overlapping bars.

The topologies in Fig. 16 were obtained with the application of the maximum filter approach with $\gamma = 0.8$, $FTol = 10^{-4}$ and the combinations of the parameters C_{Tol} = (0.0001; 0.01) and N_f = (1; 25). Figure 16 shows that all topologies formed at least two well-formed compressed arches with vertical and diagonal cables that transfer the loads to supports. This results also demonstrate that the down arches tend to have thinner bars when the objective function is controlled in every application of the filter (Fig. 16(a)) and when the application of the maximum filter is postponed, even when the objective is not controlled (Fig. 16(d)).

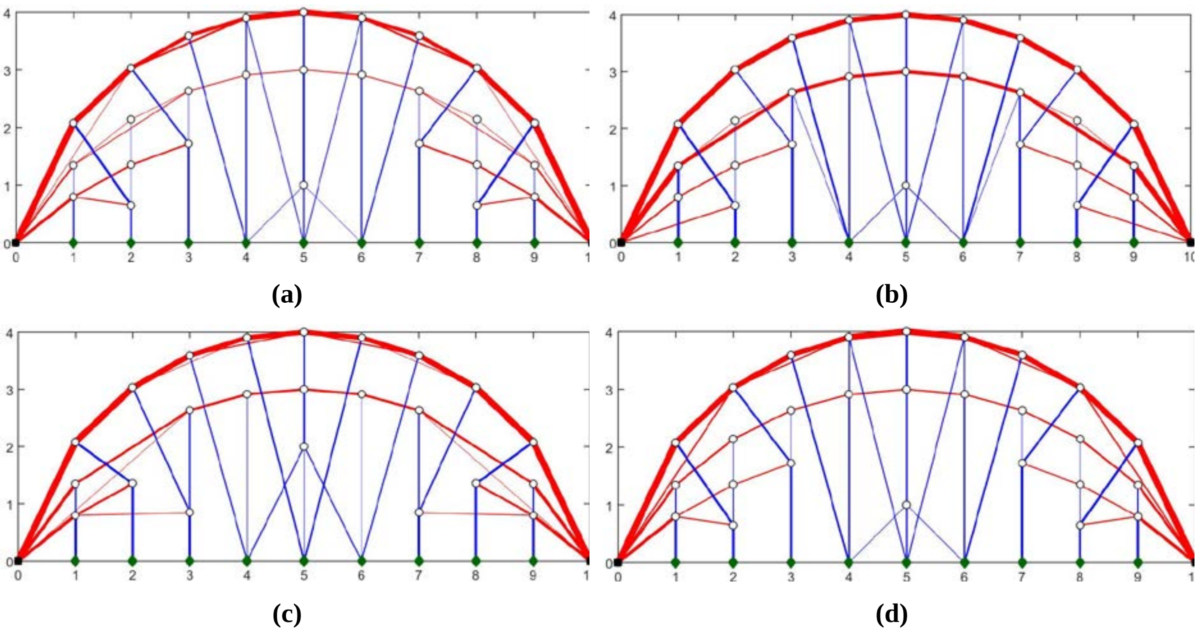

Figure 16. Final topologies of Example 3 using the maximum filter approach with: (a) C_{Tol} = 0.0001 and N_f = 1; (b) C_{Tol} = 0.0001 and N_f = 25; (c) C_{Tol} = 0.01 and N_f = 1; (d) C_{Tol} = 0.01 and N_f = 25.

4 CONCLUSIONS

Comparing the two filters for the elastic formulations, one can see that the layouts obtained using the maximum filter at each iteration conduces in general to layouts with less bars than when using the maximum filter. In the other hand, the compliance control have more effect in the final layout when using the maximum filter. The option of not applying the filter at each iteration provides interesting results, but one must carry to use a small interval N_f , otherwise the layout converges to the standard formulation.

As mentioned by Sanders et al (2017), the maximum filter used as an end filter for the plastic formulations provides good results. The improvement in the maximum filter implemented in this paper provides good time savings, especially when using small intervals N_f and high values of C_{Tol}.

ACKNOWLEDGEMENTS

The authors acknowledge CAPES and CNPq for providing financial support.

REFERENCES

Christensen, P. W., Klarbring, A., 2009. An introduction to structural optimization. Springer.

Sanders, E. D.; Ramos Jr, A. S.; Paulino, G. H., 2017. A maximum filter for the ground structure method: An optimization tool to harness multiple structural designs. *Engineering Structures*, 151, pp. 235-252.

Dorn, W.; Gomory, R.; Greenberg, H., 1964. Automatic design of optimal structures. *Journal Mecanique*, vol. 3, n. 1, pp. 25–52.

Ohsaki, M., 2010. Optimization of finite dimensional structures. CRC Press.

Ramos Jr, A. S.; Paulino, G. H., 2016. Filtering structures out of ground structures – a discrete filtering tool for structural design optimization. *Structural and Multidisciplinary Optimization*, vol. 54, n. 1, pp. 95–116.

Tikhonov AN, Arsenin VY (1977) Methods for solving Ill-posed problems.Wiley, New York.

Zegard, T.; Paulino, G. H., 2014. GRAND – Ground structure based topology optimization for arbitrary 2D domains using MATLAB. *Structural and Multidisciplinary Optimization*, vol. 50, n. 5, pp. 861–882.